TGA-FT-IR Analysis of Evolution of Oxygenated Organics by Isothermal Low-Temperature Decomposition of Rice Straw Hydrolysis Residue

Ghatak, Himadri Roy*+

Department of Chemical Engineering, Sant Longowal Institute of Engineering and Technology, Longowal, Sangrur, Punjab, INDIA

ABSTRACT: *The study presents a TGA-FT-IR analysis of low-temperature thermochemical transformations of Rice straw hydrolysis residue (RSHR). Isothermal decomposition of RSHR was carried out for 3 h, at decomposition temperatures of 200, 250, 300, and 350 °C. At 200 °C, the rate of mass loss never exceeds %1/min and except for the first five minutes, it is less than %0.5/min. The initial rate of mass loss at 250 °C is %1.6/min which quickly drops to %0.6/min in the first 10 minutes and goes on further decreasing thereafter. At 300 °C, there is a rapid initial mass loss with the initial rate peaking at %8.8/min. At 350 °C, there is an initial burst of volatiles accounting for most of the mass loss with the initial rate of mass loss being %50/min. The residual mass obtained after these runs was 81.5, 38, 24, and 15%, respectively. FT-IR spectra of evolved gases suggest that volatile oxygenated organics along with non-condensable components like CO_2, and CO are evolved during low-temperature thermal decomposition of RSHR. Carbonyls – acids, esters, aldehydes, and ketones – are the main functional groups in the volatiles. Strong absorption bands ranging 3400 – 3900 cm^{-1} indicated the presence of alcohols and phenols as other functional groups. Decomposition residues, the biochar, were demethoxylated and dehydrogenated compared to RSHR but retained their basic lignocellulosic nature.*

KEYWORDS: *Isothermal decomposition; Evolved gases; Volatiles; Biochar.*

INTRODUCTION

Rice cultivation is an important agricultural activity in India. Besides the grain, it produces an enormous amount of solid waste in the form of leftover straw. However, in their urge to quickly clear the field and prepare it for the next crop, farmers often resort to open uncontrolled burning of rice straw. The practice, needless to say, is fraught with severe environmental consequences [1,2]. The same biomass, if properly utilized, can be a valuable renewable resource. With the commitment to phase out fossil fuels, the country is earnestly looking for renewable alternatives. In this context, the National Policy on Biofuels emphasizes lignocellulosic biorefineries where leftover straw can be the raw material to produce bioethanol [3]. Govt. of India is promoting this endeavour through Viability Gap Funding and a good number of such biorefineries are in the pipeline. The first step in bioethanol production from lignocelluloses is to hydrolyse the cellulose and hemicellulose fraction

* *To whom correspondence should be addressed.*
+E-mail: hrghatak@sliet.ac.in; h_r_ghatak@yahoo.com
1021-9986/2023/11/3697-3706 10/$/6.00

to release the fermentable sugars. Acid hydrolysis is one such method [4,5] which leaves behind a substantial amount of lignin-rich solid residue. Adding value to this largely neglected biomass residue can vastly improve the economic bottom line of these biorefineries [6,7]. This is one of the main objectives of the present work.

Thermochemical transformation – pyrolysis and gasification – of biomass can yield important organic chemicals besides liquid and gaseous fuels [8]. Pyrolysis – thermochemical treatment in the absence of oxygen – of lignocelluloses is an important process choice for its value addition. Saw dust pyrolysis released volatiles including carbonyls, ethers, and amines [9]. Among the chemical components of lignocelluloses, lignin is comparatively difficult to pyrolyse [10] but yields important aromatic chemicals including phenols [11]. Catalytic pyrolysis often gives improved product yield, and the process can also be tuned to control the product composition [8,12]. Besides conventional pyrolysis at higher temperatures, thermal decomposition at low temperature-inert atmosphere is possible to get low molecular weight organics and industrially important solid residue [13]. Lignin, when subjected to Low-Temperature Thermal Decomposition (LTTD), undergoes significant chemical changes [14]. Organic acids, ketones, and phenolic compounds are released as volatiles when lignocelluloses are thermally decomposed at low temperatures [13, 15]. Notably, the higher heating value of the solid residue from wood increased markedly when thermally decomposed at 340 °C [16].

It is customary to study the thermochemical decomposition of biomass through TGA with a temperature ramp applied. Most of the industrial pyrolysers, however, work under fixed temperature conditions. The study of thermal decomposition of biomass under isothermal conditions is, therefore, important. There are numerous reports in technical literature on the thermochemical decomposition of lignocelluloses or their isolated individual components; cellulose, hemicelluloses, and lignin. On the contrary, research findings on the thermochemical decomposition of RSHR are rare and studies on its isothermal LTTD are non-existent. The present study is an analysis of the isothermal LTTD behaviour of RSHR to elucidate the mass loss pattern and evolution of major volatiles and non-condensable components. This sets apart the present work from earlier reports and opens a possible route for adding value to a waste stream from second-generation biorefineries.

EXPERIMENTAL SECTION

Materials

Rice straw, collected from a nearby farm, was washed clean of extraneous material. Post-sun drying the straw was cut into small pieces of 2 – 3 cm length. Acid hydrolysis of rice straw pieces was performed in two stages. An experimental protocol was designed based on previously reported work on acid hydrolysis of lignocelluloses [17, 18]. The reactor used was a 2 L stainless steel bomb. Initially, 100 g rice straw pieces were uniformly impregnated with dilute H_2SO_4. 1 L of 3% H_2SO_4 solution was used for impregnation. Impregnated material was heated for 20 minutes at 120 °C. The reaction bomb was cooled to room temperature. Hydrolysate from acid-treated straw was separated by hand squeezing on a 400-mesh stainless steel wire screen. Residual hydrolysate was removed from the solids by repeated water washing. The washed solid residue was again impregnated with a second serving of 1 L of 3% H_2SO_4 solution. Then the material was heated at 200 °C. for 10 minutes. Hydrolysate was separated like the first stage to get RSHR. It was stored after oven drying for TGA-FT-IR studies. The mass of oven-dried RSHR was 37.75% of the initial rice straw.

Analytical grade chemicals were sourced from S.D. Fine-chem Ltd. Deionised water from Millipore RiOS 5 Century Synergy water purifier was used for all experiments. FT-IR spectra were recorded using spectroscopy-grade potassium bromide.

Preliminary characterization

Proximate analysis conformed to ASTM D3172 standard. Moisture-free RSHR contained 63.8% volatile matter, 16.8% fixed carbon, and 19.4% ash. Klason lignin in RSHR was determined to be 72.3%, tested following TAPPI standard T 222 om-11. Holocellulose was determined by using a three-stage delignification protocol [19]. Starting material was 5 g RSHR. The delignification agent in each stage was a solution of 1.5 g sodium chlorite and 2 mL glacial acetic acid in 150 mL water. Reaction temperature was 70 °C. For each stage, delignification time was 1 h. After three stage delignification the material was water washed till acid free followed by a final wash with 50 mL acetone.

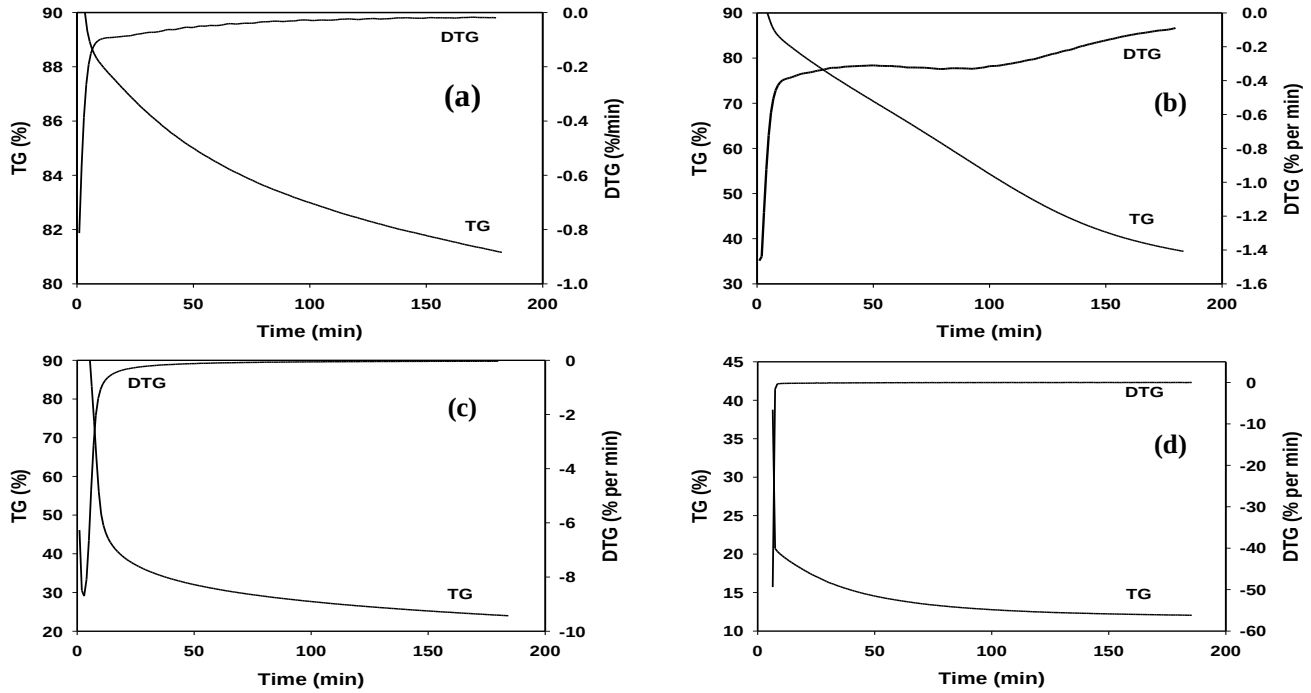

Fig. 1: Mass loss behaviour of RSHR during low temperature isothermal decomposition; (a) 200 ºC, (b) 250 ºC, (c) 300 ºC, (d) 350 ºC

Holocellulose so obtained was oven dried and weighed to be 36.9% of RSHR.

TGA-FT-IR

TGA-FT-IR studies were performed in a TG 209 F3 Tarsus (Netzsch make) thermogravimetric analyser and Tensor 27 (Bruker make) FT-IR combo. Evolved gases from TG instrument entered the gas cell of FT-IR spectroscope through a transfer line. The transfer line was maintained at an elevated temperature to avoid condensation. RSHR, about 10 mg in an alumina crucible, was thermally decomposed in 80 mL/min nitrogen flow following the desired temperature program. FT-IR spectra of evolved gases were recorded every 16 s in real-time. Wavenumber ranged from 4000 to 650 cm^{-1}, and 4 cm^{-1} was the spectral resolution. For each spectrum, 8 scans were co-added.

Solid samples were formed into spectroscopy-grade KBr pellets in 1:60 ratio. FT-IR Spectra – wavenumber range 4000 – 650 cm^{-1}, 4 cm^{-1} spectral resolution – were recorded by co-adding 32 scans.

RESULTS AND DISCUSSION

TGA of low-temperature thermal decomposition

Mass loss during isothermal decomposition at 200 ºC

Subsequent to heating to 200 ºC RSHR was maintained at this temperature for an extended period of time to study the isothermal decomposition. Fig. 1(a) shows the thermal decomposition at a constant temperature of 200 ºC. The material loses 3.55% mass in the first 30 minutes and another 1.84% in the next 30 minutes. Thereafter, about 2% mass loss is observed in the next hour. In the third hour of isothermal heating at 200 ºC only a meagre 1.25% mass is lost. Thus, even after three hours of heating, 81.5% of RSHR is left behind as residue and isothermal decomposition accounts for only 8.5% mass loss. During the entire duration of isothermal decomposition at 200 ºC the rate of mass loss never exceeds 1%/min and except for the first five minutes, it is less than 0.5%/min.

Mass loss during isothermal decomposition at 250 ºC

Similarly, RSHR was heated to 250 ºC and kept at this temperature to study the decomposition behaviour. TG and DTG behaviour of isothermal decomposition at 250 ºC is shown in Fig. 1(b). The first 10 minutes account for 5.57% mass loss followed by another 7.59% in the next 20 min. Material loses 9.55% mass in the next 30 minutes. Thus, the first hour of isothermal decomposition at 250 ºC results in a mass loss of close to 23%. In the second hour of isothermal decomposition at this temperature, an additional 19% mass loss is obtained. The mass loss in the third hour was 10.74%. After three hours of isothermal decomposition at 250 ºC 38% original material is left

behind as residue. To begin with, the rate of mass loss is 1.6%/min which drops to about 0.6%/min in the first 10 min. Thereafter, the rate of mass loss gradually tapers and reaches 0.25%/min by the end of 50 minutes. From here, we observe a marginal gain in the rate of mass loss up to 90 minutes of isothermal decomposition and it rises to about 0.3%/min. After that, the rate of mass loss goes on decreasing and reaches 0.1%/min at the end of 180 min.

Mass loss during isothermal decomposition at 300 ºC

The isothermal decomposition behaviour of RSHR post-heating to 300 ºC is shown in Fig. 1 (c). The material loses a whopping 40.37% in the first 10 minutes of isothermal decomposition at 300 ºC, and another 12.32% in the next 10 minutes. By the end of 30 minutes, it ends up losing 56% mass. For the sake of comparison, this is about 4% more than what is obtained with three hours of isothermal decomposition at 250 ºC. The next 30 minutes of isothermal decomposition at 300 ºC accounts for an additional 4.84% mass loss. Subsequently, the second and the third hour of isothermal decomposition at this temperature results in 4.28%, and 2.42% mass loss, respectively. 24% residual mass is left behind at the end of the hour period. The process of isothermal decomposition at 300 ºC starts with 6.6%/min rate of mass loss. Within 3 min, it quickly peaks to 8.8%/min. From here, the rate of mass loss almost linearly drops and reaches 2%/min after 12 minutes. The rate of mass loss keeps on decreasing, albeit gradually, and reaches a plateau of about 0.2%/min after 60 minutes.

Mass loss during isothermal decomposition at 350 ºC

By the time it reaches 350 ºC RSHR already loses 58% mass. Beyond this, its isothermal decomposition at this temperature is shown in Fig. 1 (d). Within the next five minutes, the material loses another 18% mass – more than three-fourths of the original RSHR converting into volatiles and non-condensable components. Beyond this the mass loss is less rapid, 4.41% in the next 25 minutes. At the end of one hour of isothermal decomposition at 350 ºC 17.22% of the original RSHR is left. Only an additional 1.5% mass loss is observed during the next one hour. During the third hour of isothermal decomposition at 350 ºC there is hardly any further mass loss. In the beginning, the rate of mass loss rapidly drops from a high of 50%/min to less than 1%/min. For the remaining part isothermal decomposition at 350 ºC proceeds very slowly which is because of the progressively lower amount of residual mass left behind.

Evolved gases during low-temperature thermal decomposition

Evolved gases during isothermal decomposition at 200 ºC

As already discussed above, isothermal decomposition at 200 ºC causes only a nominal mass loss. Fig. 2 (a) and 3 (a) show the real time composite 3D FT-IR spectra of the small number of evolved volatiles and the extracted spectra for 30, 60, 120, and 180 minutes. High resolution individual extracted spectra for different LTTD times are shown in Fig. S1. Three prominent absorption bands for O–H stretching are present with peaks at 3821, 3748, and 3671 cm^{-1} [15]. These come predominantly from water vapour, and to some extent from low molecular weight carboxylic acids, and methanol. Their intensities progressively increase with increased time of decomposition as shown in Fig. 4 (a). This is due to the release of chemically bound moisture and also demethoxylation of syringyl and guaiacyl structures in lignin. A faint peak for CO_2 appears at 2327 cm^{-1} in some of the spectra [8, 20]. The evolution of CO_2 during the course of isothermal decomposition at 200 ºC is interesting as shown in Fig. 4 (a). In the beginning, we notice some CO_2 production, but the evolution of CO_2 steadily declines and disappears in the interval between 55 – 70 minutes. Thereafter, small quantities of CO_2 are again detected in the evolved gases which stems from decarboxylation of the acids formed. Another noticeable feature of the evolved gases is the carbonyl band at 1771 cm^{-1}, arising from carboxylic acids [15], which is present in the spectra only for the first 30 minutes of decomposition time. Thus, some volatile carboxylic acids are generated during the initial phase of this low-temperature decomposition. The absorption band at 2191 cm^{-1} indicates the presence of CO in the evolved gases [21]. A small amount is produced in the initial phase of decomposition as depicted by its time trace in Fig. 4 (a).

Evolved gases during isothermal decomposition at 250 ºC

Fig. 2 (b) shows the real time composite 3D FT-IR spectra of the volatiles evolved during isothermal decomposition at 250 ºC. Extracted spectra for 10, 30, 60, 120, and 180 minutes are presented in Fig. 3 (b). High resolution individual extracted spectra for different LTTD times are shown in Fig. S2. Moieties containing hydroxyl

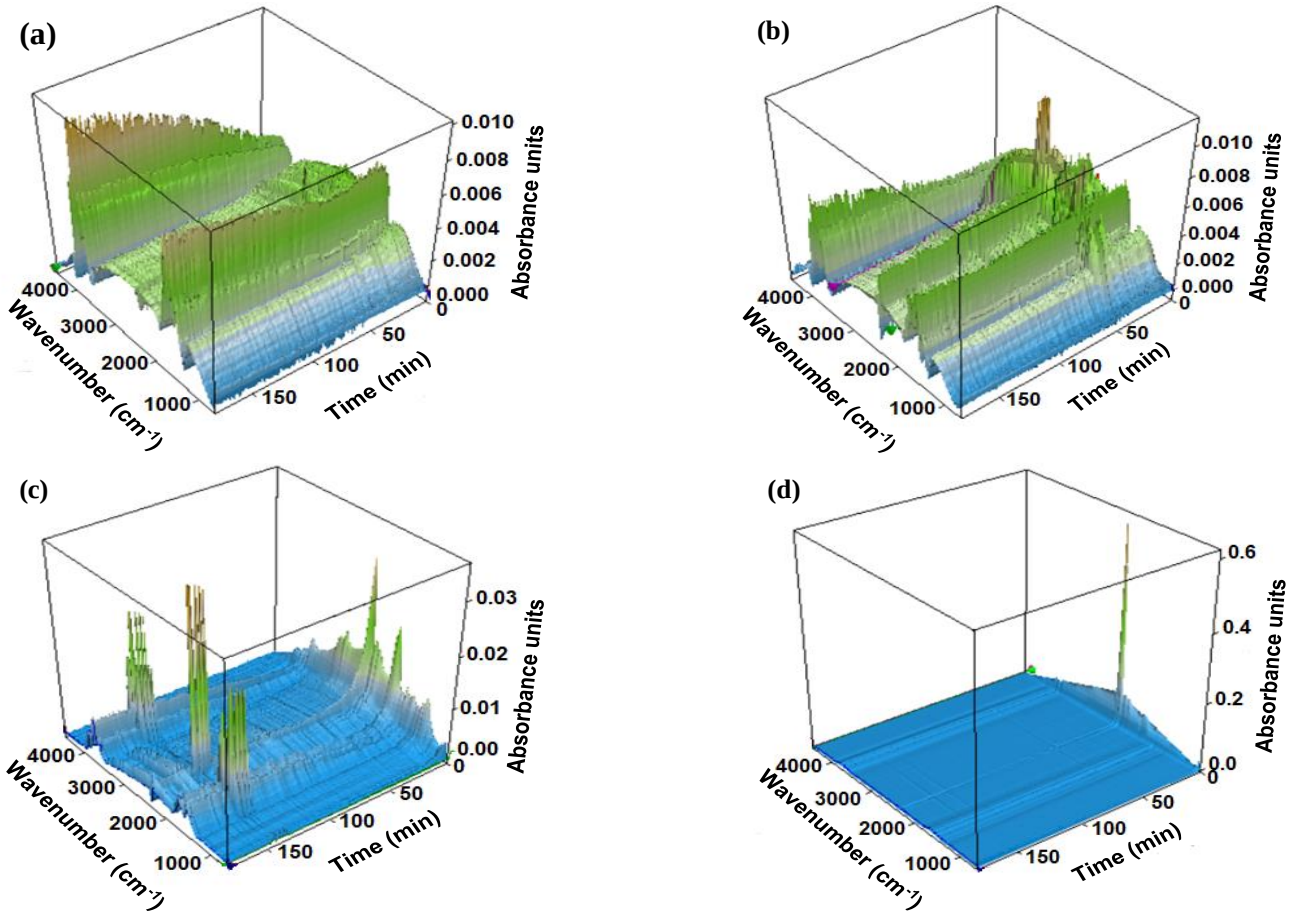

Fig. 2: Composite 3D FT-IR spectra of evolved gases during low temperature isothermal decomposition of RSHR; (a) 200 °C, (b) 250 °C, (c) 300 °C, (d) 350 °C

groups are present in the evolved volatiles throughout the decomposition as indicated by absorption peaks at 3819, 3750, and 3672 cm^{-1}. The most prominent band in the FT-IR spectra of evolved gases is due to CO_2, appearing as a doublet at 2383 and 2305 cm^{-1} and assigned to C=O stretching [20]. The weak absorption band centred at 1694 cm^{-1} is assigned to C=O stretching of aromatic aldehydes [7]. The carbonyl peak at 1772 cm^{-1}, which shows its presence for the entire duration of isothermal decomposition at 250 °C, is due to C=O stretching in phenyl esters [15].

C–O stretching bands between 1200 – 1300 cm^{-1} are present in the FT-IR spectra for all decomposition times which may be due to alcohols or phenols besides esters. Absorption peaks for methane and carbon monoxide appear at 2811 cm^{-1} (C–H stretching), and 2186 cm^{-1} (C–O stretching) [21]. There are other non-methane alkanes present as well showing absorption peaks for C–H bending at 722 cm^{-1}. The evolution of major chemical moieties with increasing time of isothermal decomposition at 250 °C is depicted in Fig. 4 (b). Organics are produced in higher amounts between 40 to 60 minutes of decomposition, peaking at about 50 minutes, as shown by their absorption intensities. This is the duration when the least amount of water vapour is released. Beyond 2 hours of decomposition time only carbon dioxide, aldehydes, and water vapour are released. It confirms that in the 60-minute to 120-minute interval RSHR undergoes significant structural changes, both chemical and morphological, though with minimal evolution of volatiles and non-condensable components.

Evolved gases during isothermal decomposition at 300 °C

Fig. 2 (c) presents the real-time composite 3D FT-IR spectra of the evolved gases during isothermal decomposition at 300 °C with the extracted spectra for 10, 20, 30, 60, 120, and 180 minutes is shown in Fig. 3 (c). High-resolution individual extracted spectra for different LTTD times are shown in Fig. S3. From the 3D spectra it is evident that the volatiles are released in two distinct

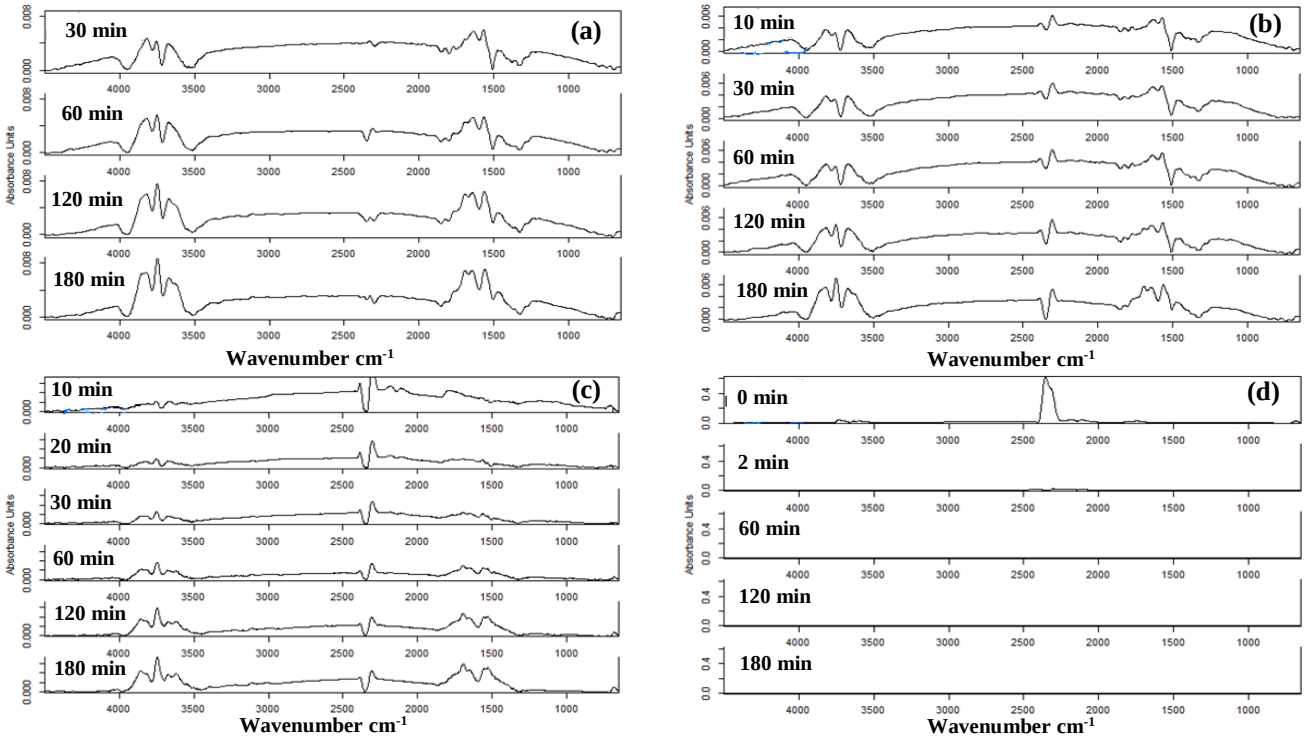

Fig. 3: Extracted FT-IR spectra of evolved gases at specific isothermal decomposition times; (a) 200 °C, (b) 250 °C, (c) 300 °C, (d) 350 °C

bursts during isothermal decomposition at 300 °C; in the first 10 minutes, and then again between 125 to 155 min. Absorption bands for water vapour between 3650–3850 cm^{-1} are similar to that observed for 250 °C decomposition. Similarly, the absorption bands for CO_2, CO, and alkanes – methane and non-methane – are also present. The carbonyl peaks are vivid in the FT-IR spectra of evolved volatiles from the isothermal decomposition of RSHR at 300 °C. In the initial period of decomposition – up to 30 minutes – absorption bands at 1790 cm^{-1}, 1770 cm^{-1}, 1736 cm^{-1}, 1700 cm^{-1}, and 1659 cm^{-1} are all present. Thus, esters, aldehydes, and ketones – non-conjugated as well as conjugated – all contribute to the product mix of evolved volatiles. With the increase in isothermal decomposition time, only two carbonyl peaks are noticed in the FT-IR spectra; a strong one at 1693 cm^{-1}, and a mild one at 1659 cm^{-1}. These are assigned to conjugated aldehydes and ketones [14, 22]. We, therefore, have aromatic aldehydes and ketones in reasonable quantities in the gases that evolve during isothermal decomposition at 300 °C. Bands at 3035 cm^{-1}, assigned to = C–H stretch of the aromatic ring, and the pair of bands at 1530 cm^{-1}, and 1487 cm^{-1}, arising from C=C stretch in the ring, confirm the presence of aromatics [14, 15]. The time traces of the evolution of the main chemical species in the evolved gases are shown in Fig. 4 (c). In the initial burst of volatile evolution, water vapour and carbonyls are less abundant while more contribution of CO_2 and CO is observed. In the second spurt of enhanced volatiles evolution between 125 – 155 minutes, there is considerable release of water vapour and carbonyls. The generation of CO_2 also spikes in this period while CO release is suppressed. This again suggests considerable chemical and morphological changes in the solids undergoing decomposition during the 20 – 125-min interval. The generation of methane is insignificant during the isothermal decomposition of RSHR at 300 °C.

Evolved gases during isothermal decomposition at 350 °C

Real-time composite 3D FT-IR spectra of the evolved gases during the isothermal decomposition of RSHR at 350 °C are shown in Fig. 2 (d). We observe the process to begin with an intense thermochemical decomposition activity and almost the entire evolution of volatiles is confined to the first 2 minutes. All the absorption bands present in the FT-IR spectra are the most pronounced at the beginning and rapidly drops thereafter. This is evident from the extracted spectra for select isothermal decomposition times as presented in Fig. 3 (d). High-resolution individual

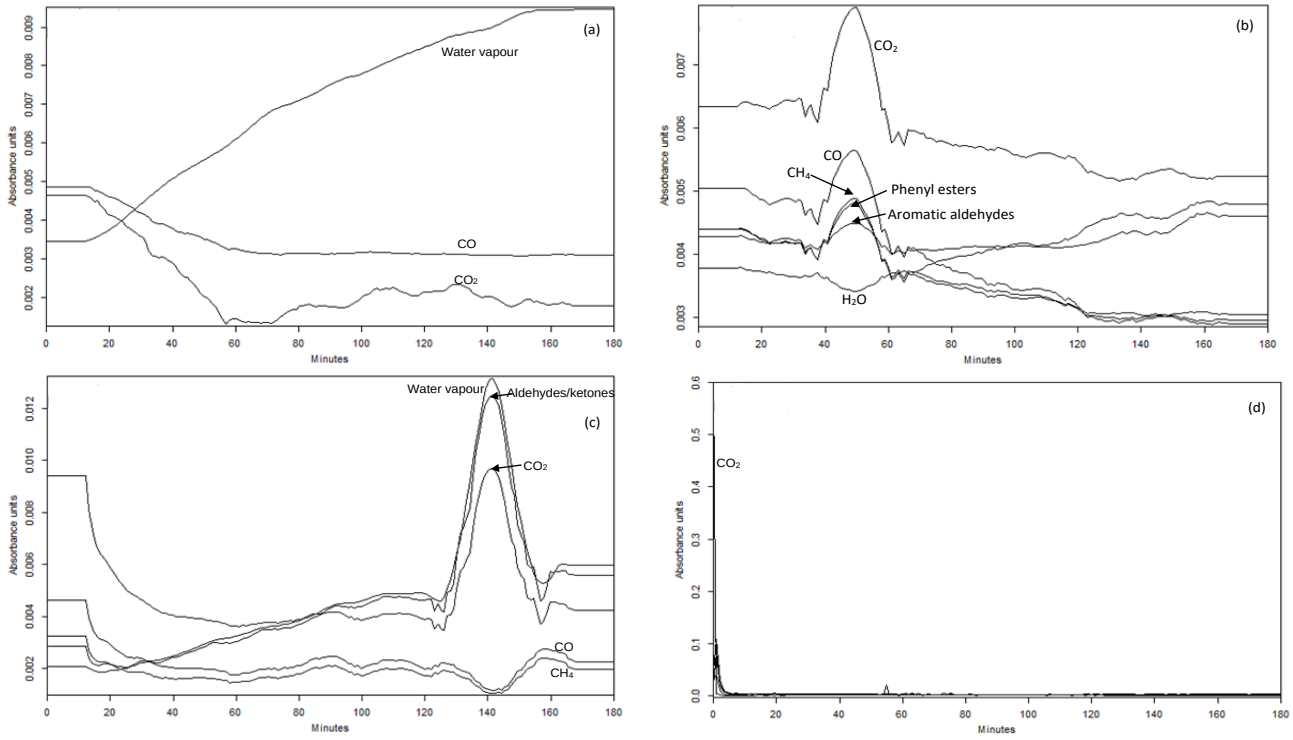

Fig. 4: Time-dependent evolution profiles of evolved gases for isothermal decomposition of RSHR; (a) 200 °C, (b) 250 °C, (c) 300 °C, (d) 350 °C

extracted spectra for different LTTD times are shown in Fig. S4. Compared to the spectrum for the start of isothermal decomposition, the peak intensities in other spectra are negligible. Even after 2 minutes decomposition time, we can notice a very sharp drop in the FT-IR absorption intensity. The major decomposition product during this initial period of volatiles evolution is carbon dioxide which makes its presence felt through a colossal band centred at 2347 cm^{-1}. All the other absorption bands, which do appear in the spectrum, have less than 10% intensity compared to the CO_2 band. CO is present, giving absorption in the FT-IR spectrum at 2180 cm^{-1}. Another notable inclusion is aromatic carbonyls showing absorption at 1752 cm^{-1} (C=O stretch) and 1517 cm^{-1} (C=C stretch in the ring). Within 2 minutes of decomposition, CO_2 intensity reduces by more than 98% and disappears in subsequent spectra. Carbon monoxide and volatile carbonyls continue to be released. The time traces of the evolution of volatiles is shown in Fig. 4 (d).

Residue from isothermal decomposition

FT-IR spectra of the solid residues left after isothermal decomposition for 3 hours at different temperatures are shown in Fig. 5. High-resolution individual spectra for RSHR and biochar residue at different LTTD temperatures are shown in Fig. S5. The absorption bands present and their assignments are presented in Table 1. Bands for O–H stretch of free hydroxyls at 3648 – 3652 cm^{-1} and those for O–H stretch of hydrogen-bonded hydroxyls at 3430 – 3431 cm^{-1} are observed in FT-IR spectra of RSHR as well as all the solid residues. Similarly, the absorption band representative of aromatic skeletal vibrations at 1588 – 1598 cm^{-1} could be noticed in all the spectra. Another absorption band at 1100 – 1108 cm^{-1}, assigned to asymmetric valence vibrations of the pyranose ring, are also to be found in all the spectra. It is, therefore, obvious that even after all the thermal degradations and mass loss the solid residues still retain to some extent the basic chemical structural features of lignin and carbohydrates – aromatic skeleton reminiscent of lignin and pyranose ring that of carbohydrates. The band corresponding to C–H symmetrical stretch of methyl is present only in RSHR and the residue from isothermal decomposition at 200 °C. In residues from higher decomposition temperatures, this band has negligible intensity. Solid residues from isothermal decomposition at 250 and 300 °C show absorption bands from olefinic C=C stretch indicating

Table 1: Major FT-IR absorption bands in RSHR and solid residues after isothermal decomposition at different temperatures. All absorption bands in cm^{-1}

RSHR	200 ºC	250 ºC	300 ºC	350 ºC	Assignment
3648	3651	3651	3652	3652	Free O–H stretch [14]
3430	3431	3431	3431	3431	H-bonded hydroxyls (lignin) [14]
3279	3265				H-bonded hydroxyls (from degraded carbohydrates [23]
		3091			=C–H stretch [14]
			3038		=C–H stretch [14]
2899	2899				C–H symmetrical stretch of methyl [22]
			1749	1749 (only shoulder)	C=O stretch in non-conjugated carbonyls in free esters [14]
		1726			C=O stretch in non-conjugated carbonyls (ketone/aldehyde in carbohydrates) [22]
1700	1700 (only shoulder)				C=O stretch in conjugated carbonyls [14,22]
1598	1588	1588	1588	1588 (only shoulder)	Aromatic skeletal vibrations with C=O stretch [22]
1553					N–H bending in amines [14]
	1522				N–H bending in amines [14]
1511					Aromatic skeletal vibrations [14]
1423					Aromatic skeletal vibrations with C–H in-plane bends [22]
1368					In-plane C–H bends [22]
1321					C–O–C stretching in guaiacyl and syringyl moieties [22]
1161	1161				C–O–C asymmetrical stretching in carbohydrates [22]
1108	1107	1100	1103	1100	Asymmetric valence vibrations of pyranose ring [15]
1062	1064				C–O stretch [14]

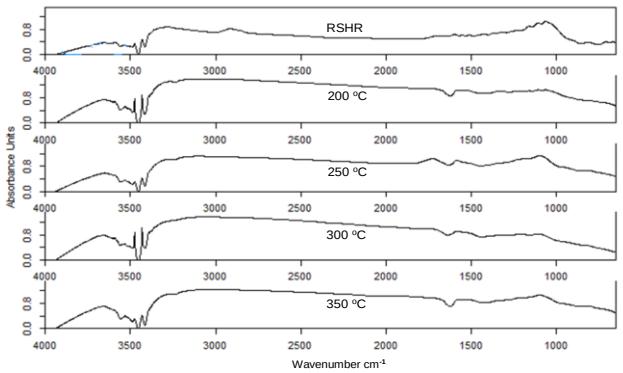

Fig. 5: FT-IR spectra of solid residues (biochar) left after isothermal decomposition at different temperatures

at 3038 – 3091 cm^{-} that dehydrogenation leading to unsaturation takes place. Carbonyl bands shift to higher frequencies with an increase in decomposition temperature. Aromatic carbonyls with conjugated C=O moieties are present in RSHR and the residue from isothermal decomposition at 200 ºC. Residues obtained from higher decomposition temperatures, however, have non-conjugated carbonyls indicating structural changes in the carbon backbone. Bands in the spectral region 1320 – 1560 cm^{-1} are only present in the FT-IR spectra of RSHR. Of these, the 1321 cm^{-1} absorption, assigned to C–O–C stretching in guaiacyl and syringyl moieties, deserves special mention. Absence of this band in the FT-IR spectra of all the solid residues points to extensive demethoxylation and cleavage of ether bonds. This also supports the absence of a band for C–H symmetrical stretch of methyl in the residues from higher decomposition temperatures.

CONCLUSIONS

With the right choice of temperature and treatment time, low-temperature isothermal decomposition is suitable for producing oxygenated organic compounds – alcohols, phenols, aldehydes, ketones, carboxylic acids, and esters – along with biochar having modified lignocellulosic character. Decomposition at 200 ºC should be suitable for producing biochar only. Decomposition at 250 ºC would predominantly result in the production of aromatic aldehydes and esters besides methane, carbon monoxide, and carbon dioxide with valuable biochar also left after the treatment. Similarly, isothermal decomposition

at 300 ºC would be suitable for producing carbonyl compounds, mainly aromatic aldehydes and ketones, in higher amounts with less production of biochar. Decomposition at 350 ºC would not be helpful for producing oxygenated organic compounds or biochar. Solid residues from LTTD retained their basic lignocellulosic nature but with extensive cleavage of ether bonds and demethoxylation. During isothermal decomposition at 250 ºC and 300 ºC, there were specific time windows in which enhanced evolution of volatiles and gaseous products was noticed. This information should be helpful in fractionation and separation of components.

Received: Aug. 16, 2023; Accepted: Sep. 25, 2023

REFERENCES

[1] Kumar P., Joshi L., "Pollution Caused by Agricultural Waste Burning and Possible Alternate Uses of Crop Stubble: A Case Study of Punjab", Springer, Berlin, 367-385 (2013)

[2] Borah N., Barua R., Nath D., Hazarika K., Phukon A., Goswami K., Barua D.C., Low Energy Rice Stubble Management Through in Situ Decomposition, *Procedia Environ. Sci.*, **35:** 771 – 780 (2016).

[3] National Policy on Biofuels, http://164.100.94.214/sites/default/files/uploads/biofuel_policy_0.pdf. Accessed 11 March 2019.

[4] Taherzadeh M.J., Karimi K., Acid-Based Hydrolysis Processes for Ethanol From Lignocellulosic Materials: A Review, *BioRes.*, **2:** 472-499 (2007).

[5] Wang C., Duan X., Wang W., Li Z., Qin Y., Establishment and Verification of A Shrinking Core Model for Dilute Acid Hydrolysis of Lignocellulose, *Front. En.*, **6:** 413–419 (2012).

[6] Chandel A.K., Garlapati V.K., Singh A.K., Antunes F.A.F., da Silva S.S., The Path Forward for Lignocellulose Biorefineries: Bottlenecks, Solutions, and Perspective on Commercialization, *Bioresource Technol.*, **264:** 370-381 (2018).

[7] Zhang Y.H.P., Reviving the Carbohydrate Economy *via* Multi-Product Lignocellulose Biorefineries, *J. Ind. Microbiol. Biotechnol.*, **35:** 367–375 (2008).

[8] Baranitharan P., Jeyabalaganesh G., Ramesh K., A Complete Characterization of Solid, Liquid and Gas Phase Products Derived from the Thermochemical Pathway of New Feedstock Grevillea Robusta Sawdust, *Iran. J. Chem. Chem. Eng. (IJCCE)* [in Press], (2023). DOI: 10.30492/IJCCE.2023.2001861.6019.

[9] Tang Y., Ma X., Wang Z., Wu Z., Yu Q., A Study of the Thermal Degradation of Six Typical Municipal Waste Components in CO_2 and N_2 Atmospheres Using TGA-FT-IR, *Thermochim. Acta*, **657:** 12–19 (2017).

[10] Chen T., Li L., Zhao R., Wu J., Pyrolysis Kinetic Analysis of the Three Pseudocomponents of Biomass–Cellulose, Hemicellulose and Lignin, *J. Therm. Anal. Calorim.*, **128:** 1825–1832 (2017).

[11] Hatakeyama H., Tsujimoto Y., Zarubin M.J., Krutov S.M., Hatakeyama T., Thermal Decomposition and Glass Transition of Industrial Hydrolysis Lignin, *J. Therm. Anal. Calorim.*, **101:** 289–295 (2010).

[12] Iliopoulou E.F., Antonakou E.V., Karakoulia S.A., Vasalos I.A., Lappas A.A., Triantafyllidis K.S., Catalytic Conversion of Biomass Pyrolysis Products by Mesoporous Materials: Effect of Steam Stability and Acidity of Al-MCM-41 Catalysts, *Chem. Eng. J.*, **134:** 51–57 (2007).

[13] Chen D., Gao A., Cen K., Zhang J., Cao X., Ma Z., Investigation of Biomass Torrefaction Based on Three Major Components: Hemicellulose, Cellulose, and Lignin, *En. Conv. Mana.*, **169:** 228–237 (2018).

[14] Reddy I.A.K., Ghatak H.R., Low-Temperature Thermal Degradation Behaviour of Non-Wood Soda Lignins and Spectroscopic Analysis of Residues, *J. Therm. Anal. Calorim.*, **132:** 407–423 (2018).

[15] Lv P., Almeida G., Perre P., TGA-FT-IR Analysis of Torrefaction of Lignocellulosic Components (Cellulose, Xylan, Lignin) in Isothermal Conditions over A Wide Range of Time Durations, *BioResources*, **10:** 4239–4251 (2015).

[16] Li M., Chen L., Li X., Chen C., Lai Y., Xiao X., Wu Y., Evaluation of the Structure and Fuel Properties of Lignocelluloses Through Carbon Dioxide Torrefaction, *En. Conv. Mana.*, **119:** 463–472 (2016).

[17] Sanchez G., Pilcher L., Roslander C., Modig T., Galbe M., Liden G., Dilute-Acid Hydrolysis for Fermentation of the Bolivian Straw Material Paja Brava, *Bioresource Technol.*, **93:** 249–256 (2004).

[18] Karimi K., Kheradmandinia S., Taherzadeh M.J. Conversion of Rice Straw to Sugars by Dilute-Acid Hydrolysis, *Biomass Bioenergy*, **30:** 247–253 (2006).
[19] Rabemanolontsoa H., Saka S., "Holocellulose Determination in Biomass", Springer, Tokyo, 135–140 (2012).
[20] Yuzbasi N.S., Selçuk N., Air and Oxy-Fuel Combustion Characteristics of Biomass/Lignite Blends in TGA-FT-IR, *Fuel Process. Technol.*, **92:** 1101–1108 (2011).
[21] Cao X., Zhong L., Peng X., Sun S., Li S., Liu S., Sun R., Comparative Study of the Pyrolysis of Lignocellulose and its Major Components: Characterization and Overall Distribution of their Biochars and Volatiles, *Bioresource Technol.*, **155:** 21–27 (2014).
[22] Xu F., Yu J., Tesso T., Dowell F., Wang D., Qualitative and Quantitative Analysis of Lignocellulosic Biomass Using Infrared Techniques: A Mini-Review, *Appl. En.*, **104:** 801–809 (2013).
[23] Fengel D., Characterization of Cellulose by Deconvoluting the OH Valency Range in FT-IR Spectra, *Holzforschung*, **46:** 283-288 (1992).